



## DEVELOPMENT OF A LABORATORY SIZE SINGLE TOGGLE JAW CRUSHER FOR ARTISANAL MINERS AND STONE WORKERS

C. Okechukwu<sup>1\*</sup>, O. A. Dahunsi<sup>2</sup>, P. K. Oke<sup>3</sup>, I. O. Oladele<sup>4</sup> and M. Dauda<sup>5</sup>

<sup>1</sup>Advanced Manufacturing Technology Programme, P. M. B. 1174, Jalingo, Taraba State, Nigeria.

<sup>2,3</sup>Department of Mechanical Engineering, Federal University of Technology, P. M. B. 704, Akure, Ondo State, Nigeria.

<sup>4</sup>Department of Metallurgical and Materials Engineering, Federal University of Technology, P. M. B. 704, Akure, Ondo State, Nigeria.

<sup>5</sup>Department of Mechanical Engineering, University of Maiduguri, P. M. B. 1069, Maiduguri, Borno State, Nigeria

\*Corresponding author's email address: [okerex2002@yahoo.com](mailto:okerex2002@yahoo.com)

### ARTICLE INFORMATION

Submitted 20 Sep., 2019

Revised 04 May, 2020

Accepted 20 May, 2020

### Keywords:

Artisanal mining,  
stone crushing,  
sustainable mineral  
processing,  
jaw crusher

### ABSTRACT

Comminution of minerals and stones in Nigeria is laden with myriads of resource challenges associated with other developing nations. A typical challenge is the need to import costly mining and mineral processing machineries or replace their components. To address this challenge, economic consideration was prominent in the development of components for the single toggle jaw crusher. Geometric modeling and structural/stress analysis of the components were achieved using Pro/Engineer<sup>®</sup> and Autodesk Inventor<sup>®</sup> computer applications. Designed eccentricity of 7 mm resulted in 5 mm throw and 0.01° angle of twist in the eccentric shaft. The designed base frame was statically stable, having yielded a maximum displacement of 0.008066 mm. Analysis of the compression spring indicated design compliance. Also, hardfaced crusher jaws and large diameter pulley and flywheel were developed. Selection of a three-phase, 3730 W electric motor resulted in a 0.24 ton/hr capacity jaw crusher in service. Optimal and maximum feed of the crusher were found to be 0.5 kg and 1 kg, respectively. Average eccentric shaft speed decreased with increased mass of granite lumps undergoing crushing. Therefore, the methods presented can be adopted in developing affordable and easily maintainable jaw crushers for artisanal miners and stone workers in Nigeria.

© 2020 Faculty of Engineering, University of Maiduguri, Nigeria. All rights reserved.

## I. Introduction

Artisanal miners and stone workers in Nigeria today still use crude tools and methods in crushing and grinding comminution processes. Wills (2006) defined comminution as the process of size reduction of particles until the liberation of valuable minerals can be achieved. Value addition in mining and minerals processing industries has always taken the route of size reduction or comminution. While ores bearing specific minerals of interest are crushed and milled to reveal and concentrate the valuable constituents, rocks which have no mineral value such as stones, e.g. granite, are crushed to particular aggregate sizes. Stone aggregates are used in structural constructions of physical infrastructures such as buildings, roads, railways, bridges, dams, harbours, airstrips, drainages, wells, walkways and parks (Asbjörnsson, 2013; Ravindran, 2013).

According to Pokrajcic (2010), comminution is the most energy intensive component of mining and mineral processing. The mineral sector accounts for about 15 % of the total electrical energy consumption in South Africa (Numbi et al., 2014). Small-scale stone crushing in underdeveloped countries is achieved through labour intensive and resource wasting activities such as breaking of the boulders using sledge and small hammers to aggregate sizes.

Interaction with stone workers during a visit to a local quarry in Jalingo, Taraba State, Nigeria, revealed that a combination of elderly men in their fifties and young men in their twenties are involved in the rock burning, boulder separation and reduction to lump sizes that the women, male and female adolescents can break into aggregates. Furthermore, women and children carry out the sieving after the manual size reduction. It takes an average of three weeks to get

a truck load (4m<sup>3</sup>) of the 31.75 mm aggregates; six weeks to get two trucks of the 31.75 mm aggregates and a pick-up vehicle load of 12.52 mm aggregates. The manual stone crushing activities in a local quarry are shown in Figure 1.



Figure 1: Adolescent children and a woman breaking stones into aggregates in Jalingo quarry, Nigeria.

Birabwa (2006) pointed out improved mechanization of small-scale stone quarrying as one of the ways to improve the livelihood of stone workers. Mohamed et al. (2014) designed a jaw crusher and advocated the need for affordable mechanized small-scale stone crushing machines. Furthermore, Alonge (2015) developed a prototype jaw crusher and identified the need for alternative and cheaper locally sourced materials for the jaws, he also called for the scaling-up of the crusher to industrial size. In addition, Elisante (2009) fabricated a jaw crusher for artisanal miners with engine prime mover but did not place adequate focus on the design and materials development for the machine's critical components.

UNDP (2014) summarily posited that there is need to bridge the gap between high capital intensity of modern mining production activities that the sector requires for significant value addition and reduction of hazard and drudgery associated with artisanal mining. This will shore up the profit of the small-scale operators, which currently dominate the sector. Access to modern technology, skills and finance are major factors in the gap that need to be addressed. Hence, this research is geared towards addressing technology and skills related challenges that are adversely affecting the profitability and sustainability of mining and minerals processing ventures in Nigeria.

Economical methods of developing critical components of the jaw crusher for easy repairs and replacement by the small-scale operators have not been adequately addressed. Towards achieving sustainable comminution, it is pertinent to unveil the procedures for developing the critical components; which include: eccentric shaft, journal bearing and hardfaced jaws. Procedures used create room for easy maintenance of the jaw crusher. Consequently, the objectives of this study are to design a 0.1 tonne/hr capacity single toggle jaw crusher; develop critical components for easy and timely reparation; develop and evaluate the performance of the jaw crusher.

## 2. Materials and Methods

### 2.1 Materials

The materials used in developing the components of the jaw crusher are presented in Table 1.

Table 1: Materials Used in Developing Hardfacing Alloys and Crusher Parts

Components	Materials
Hardfaced crusher jaws	Ferro-alloy hardfacing insert, low carbon steel
Pitman, crusher frame, rushing chamber, crushing chamber, journal bearings' housing, toggle plate, shims	Low carbon steel
Pulleys and flywheel	Grey cast iron
Eccentric shaft	Medium carbon steel

### 2.2 Design of the Single Toggle Jaw Crusher

The design of the jaw crusher commenced from the crushing compartment, through the machine elements to the selection of a prime mover.

#### 2.2.1 Determination of gape and lengths of movable jaw and pitman of the jaw crusher

Ashok and Yan model for width ( $W$ ) of the crusher jaw plate lies within the range:  $1.3G < W < 3.0G$  (Moore and Rajpal, 2013); where,  $G$  is the gape. Also, the angle of nip must lie between  $17^\circ$  and  $27^\circ$  (Niemela and Kieranen, 2008). The width of the fixed jaw,  $W = 200$  mm, the height of the fixed jaw,  $L_{fj} = 300$  mm, and the angle of nip,  $\theta = 20^\circ$ , then  $G$  can be calculated from Figure 2 as follows:

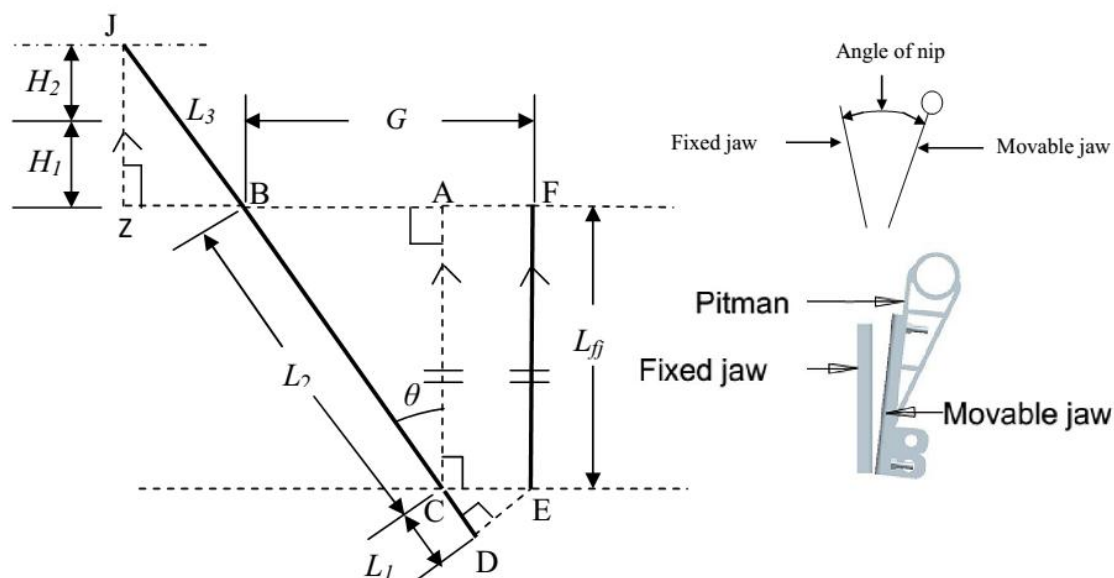


Figure 2: Schematic diagram of the crushing compartment of a single toggle jaw crusher

where,  $|BF|$  is the Gape ( $G$ ),  $|DE|$  is the Set,  $|BD|$  is the length of movable jaw,  $|JD|$  is the length of the pitman,  $H_1$  is the thickness of the journal bearing base plate, and  $H_2$  is the radius of the bearing from its centre to the surface of the base plate. From Figure 2, it can be deduced that:

$$L_2 = \frac{L_{fj}}{\cos\theta} = 319.25 \text{ mm} \quad (1)$$

Notice that  $\hat{ZJB} = \theta$  (alternate angles),  $\hat{DCE} = (180-90-\theta)^\circ = 70^\circ$  (angle on a straight line). Given that:  $H_1 = 10$  mm,  $H_2 = 70$  mm, and  $|DE| = 12.5$  mm, then:

$$L_1 = 12.5 \tan 20 = 4.55 \text{ mm}$$

Therefore, the length of the movable jaw,  $L_{mj}$  is given by:

$$L_1 + L_2 = 323.8 \approx 324 \text{ mm} \quad (2)$$

Also,  $|AF| = |CE|$ , which is given by:

$$\frac{12.5}{\sin 70^\circ} = 13.3 \text{ mm}$$

More so, the length of  $|AB|$  is given by:

$$|AB| = L_{fj} \tan \theta = 300 \tan 20^\circ = 109.2 \text{ mm}$$

This implies that the Gape,  $G$  equals

$$G = |AB| + |AF| = 109.2 + 13.3 = 122.5 \approx 123 \text{ mm.}$$

Notice that:  $1.3 \times 122.5 < 200 < 3 \times 122.5 = 159.25 < 200 < 367.5$

Hence, the width,  $W$  of the fixed jaw, which is the same as that of the movable jaw was properly selected within the range  $1.3G < W < 3.0G$ .

Additionally,

$$\begin{aligned} L_3 &= \frac{H_1 + H_2}{\cos \theta} \\ &= \frac{10 + 70}{\cos 20^\circ} = 85.13 \text{ mm} \end{aligned} \quad (3)$$

Hence, the length of pitman,  $L_p$  is given by:

$$L_p = L_1 + L_2 + L_3 \quad (\text{mm}) \quad (4)$$

By substitution,

$$L_p = 4.55 + 319.25 + 85.13 = 408.93 \approx 409 \text{ mm}$$

### 2.2.2 Determination of components of the crushing force contributed by the pitman, movable jaw, toggle plate and drawback rod

Using the density of steel,  $7.85 \text{ g/cm}^3$ , the weights of pitman-movable jaw sub-assembly ( $W_p$ ), toggle plate ( $W_T$ ) and drawback rod ( $W_R$ ) were determined with Pro/Engineer® software as 250.07 N, 31.06 N, and 28.95 N, respectively. The components of the crushing force contributed by movable jaw, toggle plate and drawback rod were determined from Figure 3:

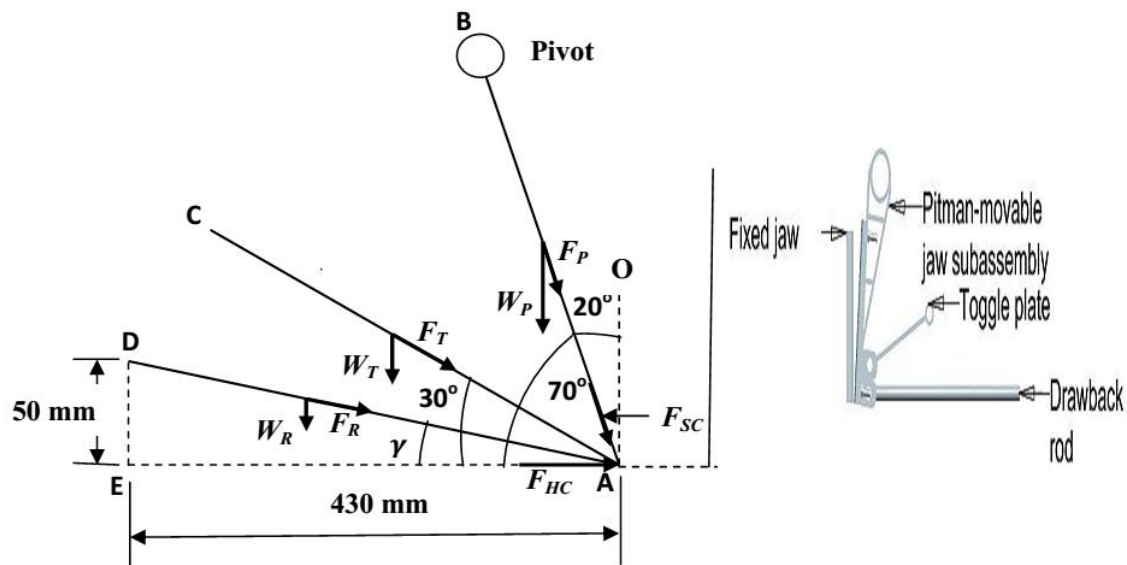


Figure 3: Contributions of the pitman, movable jaw, toggle plate and drawback rod to the crushing force

where,  $W_P$ ,  $W_T$ , and  $W_R$  were the weights of the pitman-movable jaw sub-assembly, toggle plate and drawback rod, respectively. Also,  $F_P$ ,  $F_T$  and  $F_R$  are the forces acting along the length of the pitman-movable jaw sub-assembly, toggle plate, and drawback rod due to their weights, respectively.  $F_{SC}$  is the slanted component of the crushing force along the movable jaw, while  $F_{HC}$  is the horizontal component of  $F_{SC}$ . The movable jaw is inclined at  $20^\circ$  to the vertical line /AO/, while the toggle plate is inclined at  $30^\circ$  to the horizontal line /AE/. The angle of inclination of the drawback rod is calculated thus:

$$\gamma = \tan^{-1}\left(\frac{50}{430}\right) = 6.63^\circ$$

From Figure 3,  $F_P$ ,  $F_T$  and  $F_R$  and their horizontal components  $F_{PX}$ ,  $F_{TX}$  and  $F_{RX}$ , respectively, can be calculated as follow:

$$F_P = \frac{W_P}{\sin 70^\circ} = \frac{250.07}{0.9397} = 266.12 \text{ N}$$

$$F_{PX} = F_P \cos 70^\circ = 91.02 \text{ N}$$

Similarly,

$$F_T = \frac{W_T}{\sin 30^\circ} = 62.12 \text{ N}$$

$$F_{TX} = F_T \cos 30^\circ = 53.80 \text{ N}$$

Likewise,

$$F_R = \frac{W_R}{\sin 6.63^\circ} = 250.65 \text{ N}$$

$$F_{RX} = F_R \cos 6.63^\circ = 248.97 \text{ N}$$

The horizontal component of the crushing force is given by:

$$F_{HC} = F_{PX} + F_{TX} + F_{RX} \text{ (N)} \quad (5)$$

By substitution,

$$F_{HC} = 91.02 + 53.80 + 248.97 = 393.79 \text{ N}$$

The slanted component of the crushing force along the pitman-movable jaw subassembly is given by:

$$F_{SC} = \frac{F_{HC}}{\cos 70^\circ} = 1151.43 \text{ N}$$

Furthermore, the contribution of the pulley-eccentric shaft-flywheel subassembly is as follows: Given that: mass of grey cast iron pulley is 18.4 kg, mass of grey cast iron flywheel equals 18.4 kg, and mass of medium carbon steel eccentric shaft is 13.211 kg; then, mass of pulley-eccentric shaft-flywheel =  $18.40 + 18.40 + 13.211 = 50.01$  kg, weight of pulley-eccentric shaft-flywheel sub-assembly,  $W_{PF} = 500.10$  N; this can be resolved to the slanted crushing force direction as shown in Figure 4:

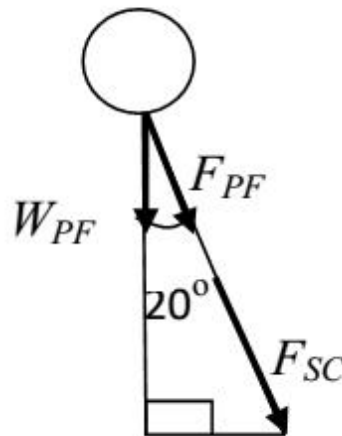


Figure 4: Contributions of the pulley, eccentric shaft and flywheel to the crushing force

From Figure 4,  $F_{PF}$  can be calculated as follows:

$$F_{PF} = \frac{W_{PF}}{\cos 20^\circ} = 532.19 \text{ N}$$

where,  $F_{PF}$  is the component of the crushing force from pulley, eccentric shaft and flywheel. Therefore, total force available along the pitman-movable jaw sub-assembly for crushing is given by:

$$F_{CF} = F_{PF} + F_{SC} \text{ (N)} \quad (6)$$

Substituting the values of  $F_{PF}$  and  $F_{SC}$  into equation (6), gives

$$F_{CF} = 1151.43 + 532.19 = 1683.62 \text{ N}$$

### 2.2.3 Estimation of power required by the jaw crusher to crush a given feed

According to Zhang (2014), the power required to crush a given feed size of ore or stone to product,  $P_R$  (kW), is given by the modified Bond's equation:

$$\frac{P_R}{\dot{m}} = 0.3161 W_i \left( \frac{1}{\sqrt{D_p}} - \frac{1}{\sqrt{D_f}} \right) \left( \frac{\text{kWhr}}{\text{tonne}} \right) \quad (7)$$

Given that: material to be crushed is granite,  $D_f = 100 \text{ mm}$ ,  $D_p = 12.5 \text{ mm}$ ,  $\dot{m} = 0.1 \text{ ton/hr}$ ,  $W_i = 15.83 \text{ kWhr/ton}$  (Kelly and Spottiswood, 1982), then,  $P_R$  (kW) can be calculated as:

$$P_R = 0.1 \times 0.3161 \times 15.83 \times \left( \frac{1}{\sqrt{12.5}} - \frac{1}{\sqrt{100}} \right) = 91.57 \text{ W}$$

Also, the reduction ratio,  $RR$  is given by:

$$RR = \frac{\text{Size of feed (mm)}}{\text{Size of product (mm)}} \quad (8)$$

By substitution,

$$RR = \frac{100}{12.5} = 8:1$$

### 2.2.4 Estimation of power available from the crushing force and eccentric shaft

The eccentricity,  $e$ , of the eccentric shaft can be determined from Figure 5 as the difference between the radii of 60 mm diameter and 74 mm diameter parts of the shaft; hence,  $e = 7$  mm.

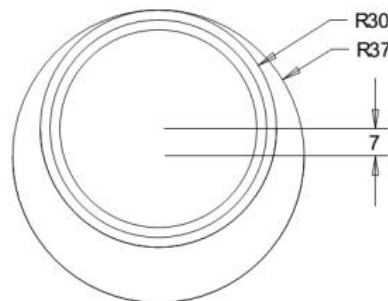


Figure 5: End view of the eccentric shaft.

The throw or stroke of the pitman-movable jaw sub-assembly is given by the difference between the eccentricity (7 mm) and the difference between the internal diameter of eccentric shaft housing (76 mm) and the diameter of the eccentric lobe (74 mm); hence,

$$\text{Stroke} = 7 - (76 - 74) = 7 - 2 = 5 \text{ mm}$$

The crusher stroke is the displacement of jaw between the widest and narrowest points on an eccentrically gyrating cycle (Karra *et al.*, 1992). Alternatively, Donovan (2003) defined the throw as the stroke of the swing jaw or the difference between the open side set and the closed side set. The open side set is the maximum discharge aperture, while the closed side set is the minimum discharge aperture.

Open side set = 15 mm; Closed side set = 10 mm

Stroke = 15 – 10 = 5 mm; Set = aggregate product size = 12.5 mm

According to Karra *et al.* (1992), the mechanical power required to drive the crushing mechanism can be calculated from equation (9) as follows:

$$\text{Horsepower} = F_{CF} \cdot x \cdot N \quad (9)$$

Let, crushing force,  $F_{CF} = 1683.62$  N, stroke,  $x = 0.005$  m, shaft speed in r.p.m.,  $N = 400$  r.p.m.

$$\begin{aligned} \text{Eccentric shaft speed} &= \frac{2\pi N}{60} \text{ (rad/s)} \\ &= 41.89 \text{ rad/s} \end{aligned} \quad (10)$$

The amount of power consumed during crushing (i.e. driving the mechanism) is calculated thus:

$$P_C = 1683.62 \times 0.005 \times 41.89 = 352.63 \text{ W}$$

### 2.2.5 Estimation of reaction forces at the bearings

Let, weight of the eccentric shaft be  $W_E = 132.11$  N, Vertical component of slanted force,  $F_{SC}$ , be  $W_{SC}$ ,

$$W_{SC} = F_{SC} \cos 20^\circ = 1151.43 \times 0.9396 = 1081.88 \text{ N}$$

Also, let reaction at each bearing support be  $R_B$ , weight of pulley,  $W_L = 184$  N, weight of flywheel,  $W_F = 184$  N. Then,  $R_B$  can be determined from the force diagram shown in Figure 6 as follows:

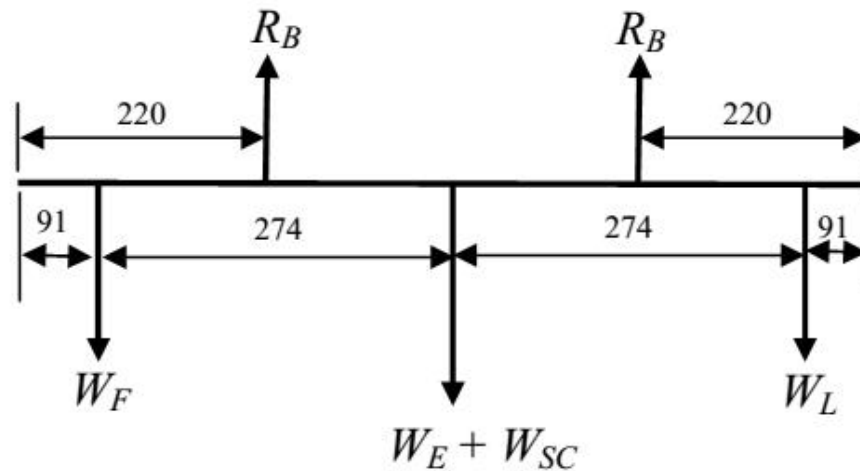


Figure 6: Force diagram for the calculation of reactions at the journal bearings.

Note: All distance dimensions in Figure 6 are in mm.

Summing vertical forces, we have:

$$R_B + R_B - W_F - W_E - W_{SC} - W_L = 0 \quad (11)$$

By substitution, we have:

$$2R_B = 184 + 132.11 + 1081.88 + 184 = 1581.99$$

$$R_B = 790.995 \sim 791 \text{ N}$$

### 2.2.6 Design of flywheel

Let,  $m_f$  be the mass of the flywheel, then,  $m_f = 18.40$  kg, speed of flywheel,  $N_f = 400$  rpm, angular speed of the flywheel is given by:

$$\omega_f = \frac{2\pi N_f}{60} \text{ (rad/s)} \quad (12)$$

By substitution,

$$\omega_f = 2 \times 3.142 \times \frac{400}{60} = 41.89 \text{ (rad/s)}$$

Radius of gyration,  $r_g$  is taken as the mean radius of the rim, because the thickness of the rim is very small compared to its diameter (Khurmi and Gupta, 2005);  $r_g$  is calculated from Figure 7 as follows:

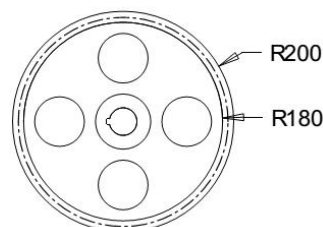


Figure 7: Schematic drawing of the flywheel for the calculation of the mean radius

$$r_g = \frac{200 + 180}{2} = 0.19 \text{ m}$$

Mass moment of inertia of the flywheel about the axis of rotation,  $I$  is given by:

$$I = m_f r_g^2 \text{ (kgm}^2\text{)} \quad (13)$$

$$= 0.66 \text{ kgm}^2$$

Mean kinetic energy of the flywheel,  $E_f$  is given by:

$$E_f = \frac{1}{2} I \omega_f^2 = \frac{1}{2} m_f r_g^2 \omega_f^2 \text{ (J)} \quad (14)$$

$$= 582.80 \text{ J}$$

Maximum fluctuation of energy,  $\Delta E_f$ , is given by:

$$\Delta E_f = I\omega_f^2 C_f = m_f r_g^2 \omega_f^2 C_f = 2E_f C_f \quad (J) \quad (15)$$

According to Khurmi and Gupta (2005), coefficient of fluctuation of speed,  $C_f$ , for crushing machines is 0.2. Hence,

$$\Delta E_f = 2 \times 582.8 \times 0.2 = 233.12 \text{ J}$$

Energy consumed per second due to the inertia of the flywheel,  $P_f = 233.12 \text{ W}$ .

Then, power required to drive the crushing mechanism and reduce the feed to product, i.e. reduce 100 mm granite feed to 12.5 mm is the sum of  $P_R$ ,  $P_C$  and  $P_f$ .

Therefore, total power consumed during crushing is given by:

$$\begin{aligned} P_{PC} &= P_R + P_C + P_f \\ &= 677.32 \text{ W} \end{aligned} \quad (16)$$

### 2.2.7 Selection of prime mover for driving the crushing mechanism

Given that:  $R_1$  is the radius of the driving or driver pulley (m),  $R_2$  is the radius of the driven or follower pulley (m),  $D_1$  is the diameter of the driver pulley (m),  $D_2$  is the diameter of the driven pulley (m),  $N_1$  is the speed of the driver pulley (r.p.m.),  $N_2$  is the speed of the driven pulley (r.p.m.),  $V_1$  is the velocity of the belt while passing driver pulley (m/s),  $V_2$  is the velocity of the belt while passing driven pulley (m/s),  $T_1$  be the tension of the tight side of the belt (N) and  $T_2$  is the tension on the slack side of the belt (N).

According to Khurmi and Gupta (2005); Juvinall and Marshek (2012), the angle of contact or lap on the large diameter driven pulley is given by:

$$\theta_2 = (180^\circ + 2\alpha) \frac{\pi}{180} \text{ (rad.)} \quad (17)$$

$$\alpha = \sin^{-1} \left( \frac{R_2 - R_1}{X} \right) \text{ (}^\circ\text{)} \quad (18)$$

where,  $X$  is the centre to centre distance between the driver shaft and the driven shaft, (m).

Then,

$$V_1 = \frac{\pi D_1 N_1}{60} \text{ (m/s)} \quad (19)$$

$$V_2 = \frac{\pi D_2 N_2}{60} \text{ (m/s)} \quad (20)$$

If there is no slip,  $V_1$  equals  $V_2$ , which implies the velocity ratio of the belt is given by:

$$\frac{N_1}{N_2} = \frac{D_2}{D_1} \quad (21)$$

The ratio of the tight side tension ( $T_1$ ) to that of the slack side tension ( $T_2$ ) is given by the expression,

$$\frac{T_1}{T_2} = e^{\mu\theta_2 \csc\beta} \quad (22)$$

where,  $\mu$  is coefficient of friction between the belt and the pulley, which equals 0.3 for cast iron and rubber belt.  $\beta$  equals half of the angle formed by the slanted sides of the V-belt or the grooved pulley. From the Pro/Engineer<sup>®</sup> software,  $2\beta = 33.86^\circ$  which implies,  $\beta = 16.93^\circ$ .

The effective turning force at the circumference of the driven pulley is the difference between the two tensions, i.e.,

$$\text{Effective turning force} = (T_1 - T_2) \quad (\text{N}) \quad (23)$$

Therefore, power transmitted by a belt is given by:

$$P_B = (T_1 - T_2)V_B \quad (\text{W}) \quad (24)$$

Torque exerted on the driven pulley equals torque transmitted by the eccentric shaft and can be calculated from the equation:

$$T_{P2} = (T_1 - T_2)R_2 \quad (\text{N.m}) \quad (25)$$

Output power available at the driven pulley is given by:

$$P_{PC} = \frac{2\pi N_2 T_{P2}}{60} \quad (\text{W}) \quad (26)$$

Input power transmitted from the prime mover is given by:

$$P_M = P_B \times n_B \quad (\text{W}) \quad (27)$$

where,  $n_B$  is the number of belts.

Efficiency of the pulley-drive system is given by:

$$\eta = \frac{\text{Output power}}{\text{Input power}} \quad (28)$$

Given that:  $P_{PC} = 677.32 \text{ W}$ ,  $D_2 = 0.4 \text{ m}$ ,  $D_1 = 0.102 \text{ m}$ ,  $R_1 = 0.2 \text{ m}$ ,  $R_2 = 0.051 \text{ m}$ ,  $\beta = 16.93^\circ$ ,  $\mu = 0.3$ ,  $X = 0.666227 \text{ m}$  and  $N_2 = 400 \text{ r.p.m.}$ , then, from equation (18),

$$\alpha = \sin^{-1} \left( \frac{0.2 - 0.051}{0.666227} \right) = 12.92^\circ$$

Also, from equation (17),

$$\theta_2 = (180^\circ + 2 \times 12.92) \times \frac{3.142}{180} = 3.593 \text{ rad.}$$

This implies that:

$$\mu\theta_2 \text{cosec}\beta = 0.3 \times 3.653 \times \text{cosec } 16.93^\circ = 3.702$$

Then, from equation (22),

$$\frac{T_1}{T_2} = e^{\mu\theta_2 \text{cosec}\beta} = e^{3.702} = 40.53$$

Hence,

$$T_1 = 40.53T_2 \quad (\text{N}) \quad (29)$$

More so, from equation (26), torque on the driven pulley can be calculated as follows:

$$T_{P2} = \frac{60P_{PC}}{2\pi N_2} = \frac{60 \times 677.32}{2 \times 3.142 \times 400} = 16.17 \text{ Nm}$$

From equations (23) and (25), the effective turning force is given by:

$$T_1 - T_2 = \frac{T_{p2}}{R_2} = \frac{16.17}{0.2} = 80.85 \text{ N}$$

Hence,

$$T_1 = 80.85 + T_2 \quad (\text{N}) \quad (30)$$

Equating equation (29) to equation (30), gives

$$\begin{aligned} 40.53T_2 &= 80.85 + T_2 \\ T_2 &= \frac{80.85}{39.53} = 2.05 \text{ N} \end{aligned}$$

Therefore,

$$T_1 = 80.85 + 2.05 = 82.90 \text{ N}$$

The speed of the driver pulley can be determined from equation (21) as follows:

$$N_1 = \frac{N_2 D_2}{D_1} = \frac{400 \times 0.4}{0.102} = 1568.63 \text{ r.p.m.}$$

Velocity of belt,  $V_1 = V_2 = V_B$  is calculated thus:

$$V_B = \frac{\pi D_1 N_1}{60} = \frac{3.142 \times 0.102 \times 1568.63}{60} = 8.38 \text{ m/s}$$

Power transmitted by a belt is calculated as follows:

$$P_B = (T_1 - T_2) V_B = 80.85 \times 8.38 = 677.52 \text{ W}$$

Most crushing mechanisms are driven with a minimum of two belts, since the crusher to be developed is of laboratory size, two belts were selected. Given that:  $n_B = 2$ ,  $P_B = 677.52 \text{ W}$ , substituting these values into equation (27), gives

$$P_M = 677.52 \times 2 = 1355.04 \text{ W}$$

Efficiency of the pulley-driven system is determined thus:

$$\eta = \frac{\text{Output power}}{\text{Input power}} = \frac{677.32}{1355.04} = 0.4999 \sim 0.5 = 50\%$$

Considering power losses due to friction, inertia forces, voltage drop, heat and vibration, the power rating of the prime mover can be taken as two and half times input, i.e.,

$$\text{Power rating of prime mover} = 2.5 \times 1355.04 = 3387.60 \text{ W}$$

At this stage, decision was made to use an electric motor as the prime mover and the selection criteria are outlined below:

Speed should be normal at about 1600 r.p.m.

Torque should be greater than the output torque of 16.8 Nm.

Power output should be at least 3.4 kW.

It must be a three-phase A.C. motor.

Based on the criteria above, the motor bought has the following specifications: Power rating = 5 hp =  $5 \times 746 = 3730 \text{ W}$ , speed = 1600 r.p.m., torque = 22.26 Nm, number of phases = 3.

### 2.3 Stress Analysis of the Components of the Jaw Crusher

Stress analysis of the eccentric shaft, base frame and spring were carried out with Autodesk Inventor® as outlined by Waguespack (2014).

### 2.3.1 Stress analysis of the eccentric shaft

Given that the shaft material is medium carbon steel, with modulus of elasticity,  $E = 206000$  MPa, modulus of rigidity,  $G_r = 80000$  MPa, density,  $\rho = 7860$  kg/m<sup>3</sup>, radial load = 184 N, continuous load on the eccentric shaft =  $1151.43$  N /  $200$  mm =  $5.757$  N/mm, direction of the continuous load =  $20^\circ$ , and torque =  $22$  Nm. Using these values and machine elements' positions shown in Figure 8, the stress analysis of the eccentric shaft was achieved.

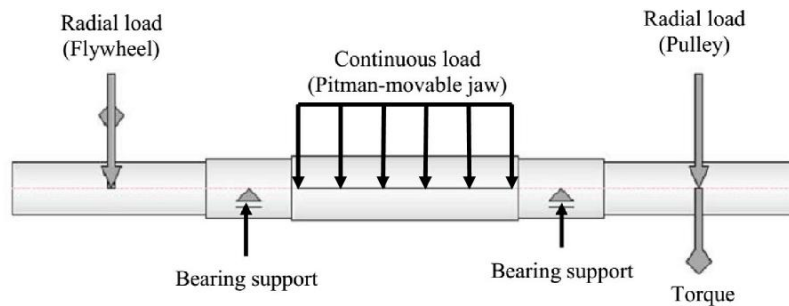


Figure 8: Positions of radial loads, bearing and continuous load on the eccentric shaft

### 2.3.2 Stress analysis of the base frame

The base frame was drawn and welded in Autodesk Inventor®, prior to the stress analysis. Fixed joints and constrained points are shown in Figure 9. Additionally, the weights of the crushing chamber and its accessories were determined, divided into six and distributed as illustrated in Figure 10, while the weight of the motor-small pulley sub-assembly was determined, divided by four and distributed as presented in Figure 11.

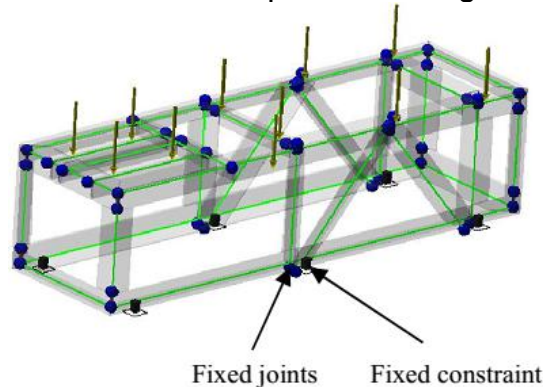


Figure 9: Fixed joints and constrained points on the base frame

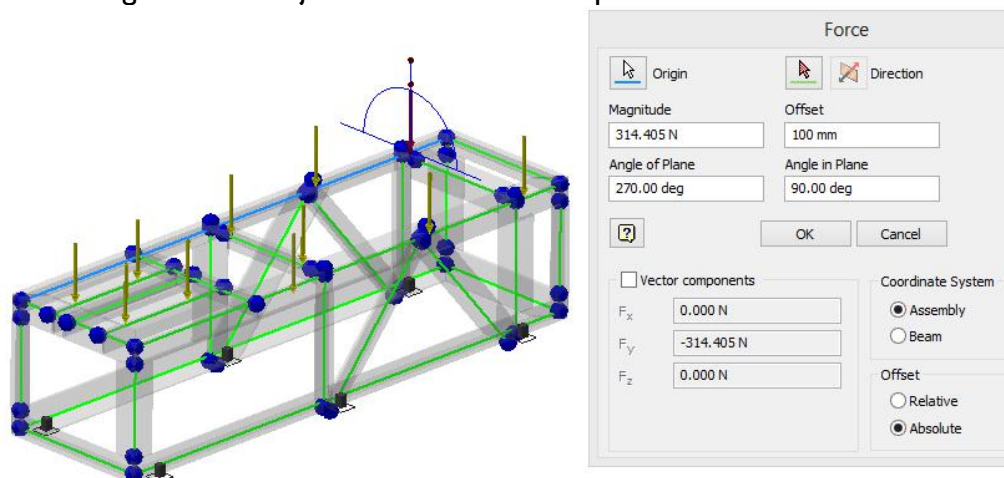


Figure 10: One-sixth of the weight of crushing chamber and its accessories

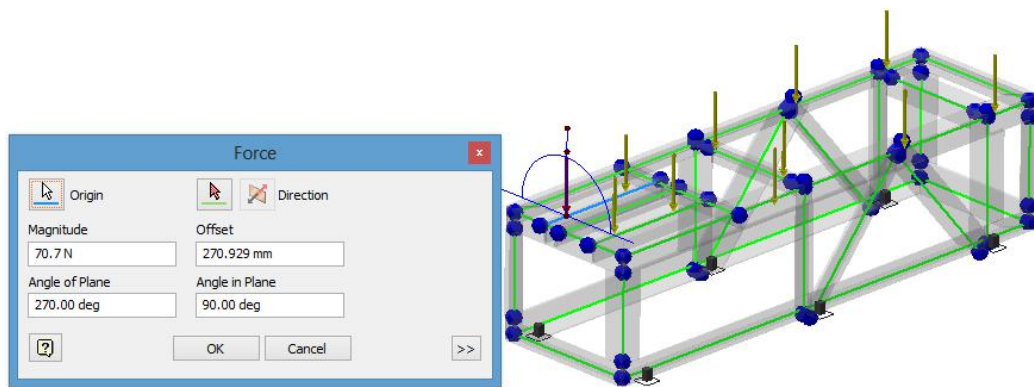


Figure 11: One-fourth of the weight of the motor-small pulley sub-assembly

### 2.3.3 Design of the compression spring

Springs are designed to provide a push, a pull, or a twist force (torque), or to primarily store energy. The spring index is the ratio of the mean coil diameter to the wire diameter; the preferred range of the spring index is from 4 to 12. If the spring index is less than 4, the spring is difficult to manufacture, when the index is greater than 12, it is prone to buckling and also tangles easily when handled in bulk (Norton, 2000).

Properties of the heat-treated wire carbon steel spring that was analysed in Autodesk Inventor® are listed in Figure 12. The spring check analysis was carried out with the minimum load as the horizontal component of the crushing force, while the working load is the component of the horizontal component when resolved along the drawback rod or at  $6.63^\circ$ .

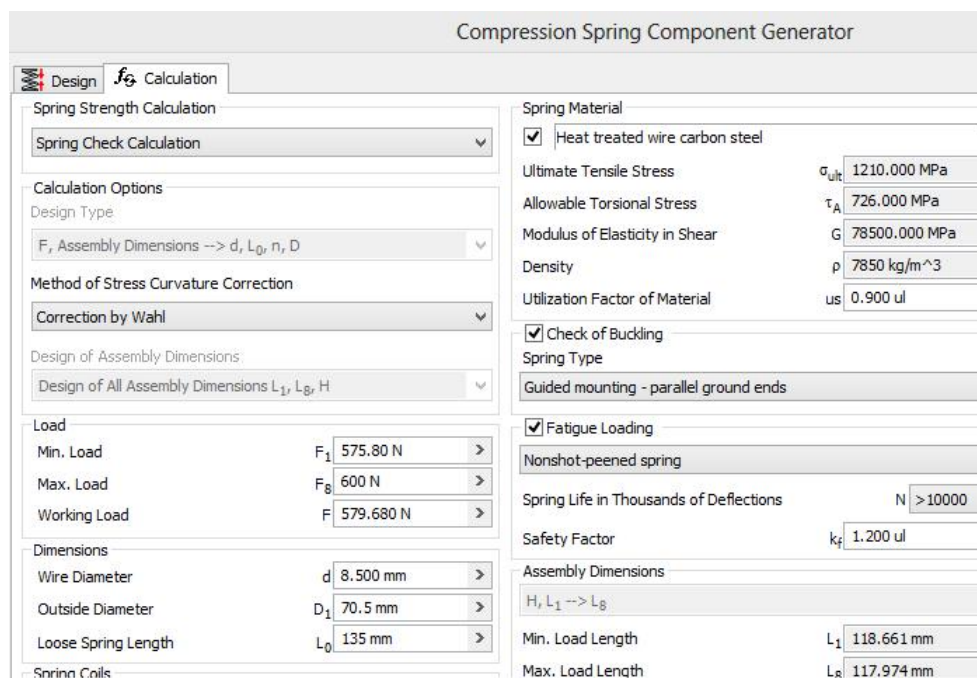


Figure 12: Properties of the compression spring

## 2.4 Development of the Eccentric Shaft

Using a medium carbon steel shaft of  $\text{Ø}74$  mm, the following dimensions were considered prior to production of the eccentric shaft by machining: diameter of the hole in hubs of the large diameter pulley and flywheel = 50 mm, diameter of the bearing bore = 55 mm, eccentric lobe diameter = 74 mm and stopper diameter = 60 mm. The working drawings of the machining steps 1 to 9, taken towards producing the eccentric shaft are presented in Figure 13 to Figure 22. The machining steps are as follow:

- Step 1: A straight line was drawn through the centre of the ends of the  $\text{Ø}74$  mm solid shaft and along its length;
- Step 2: An offset of 30 mm was marked from the opposite ends of the shaft and each point was centre-punched;
- Step 3: A hole was drilled at one end of the centre-punched point; with a radius of 25 mm, a circle was drawn with its centre at 30 mm from the edge of the opposite circular end;
- Step 4: About 100 mm length of a  $\text{Ø}50$  mm shaft was turned on the lathe and its circular end welded to the  $\text{Ø}50$  mm circle on one end of the  $\text{Ø}74$  mm shaft;
- Step 5: The attached  $\text{Ø}50$  mm shaft was mounted in the jaw chuck of the lathe and the other centre-punched end on the tailstock; the job was set with the aid of a tool;
- Step 6: 200 mm length was marked-out at 265 mm offset from the tailstock end; with a cut of 0.5 mm, shaft was step-turned to  $\text{Ø}60$  mm from the both ends of the 200 mm lobe and parallel-turned to the ends of the shaft;
- Step 7: An offset of 5 mm was marked out from both ends of the 200 mm lobe, step-turned to  $\text{Ø}55$  mm from the  $\text{Ø}60$  mm and parallel-turned to the ends of the shaft;
- Step 8:  $\text{Ø}50$  mm was step-turned at 80 mm from 5 mm offset, and parallel-turned 180 mm on the tailstock side and 200 mm on the headstock side; and
- Step 9: Unclamp the machined part and part-off of the welded part.

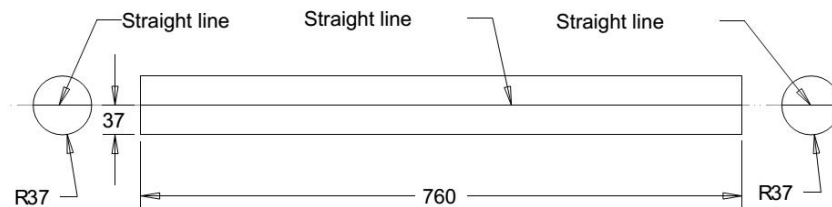


Figure 13: Geometric model of machining step 1

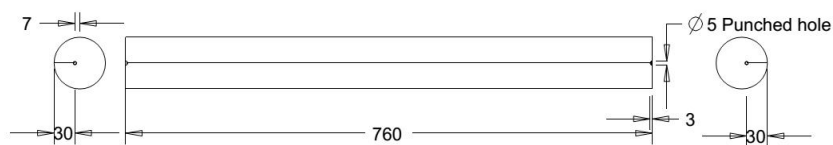


Figure 14: Geometric model of machining step 2

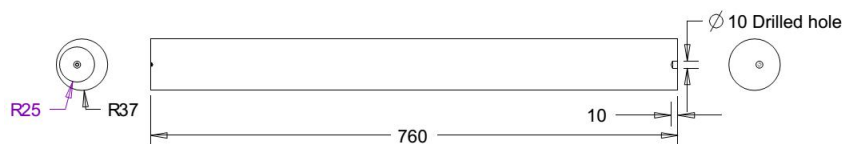


Figure 15: Geometric model of machining step 3

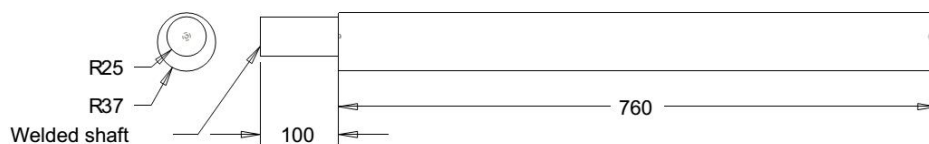


Figure 16: Geometric model of machining step 4

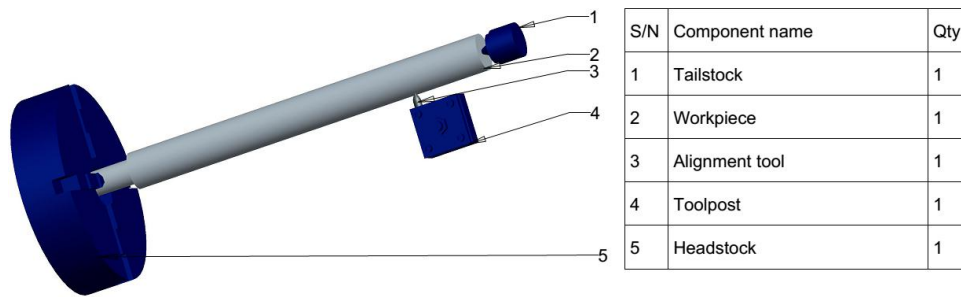


Figure 17: Geometric model of machining step 5

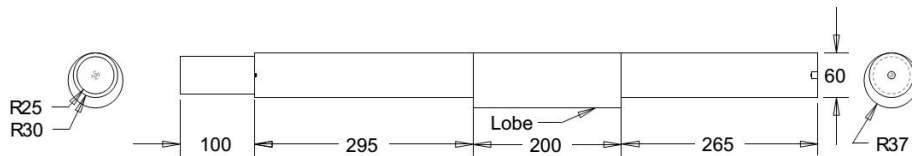


Figure 18: Geometric model of machining step 6

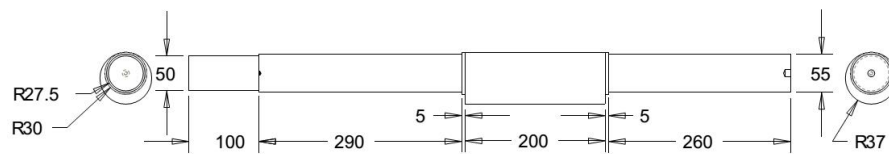


Figure 19: Geometric model of machining step 7

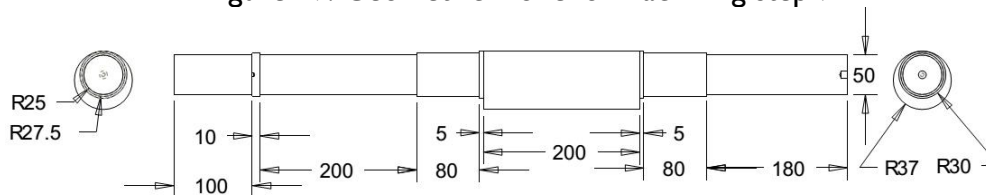


Figure 20: Geometric model of machining step 8

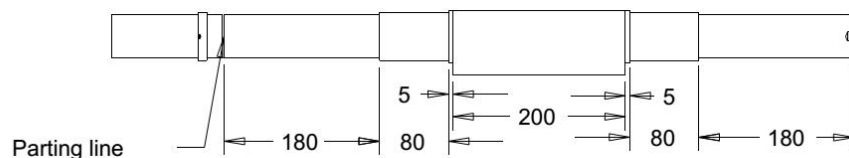


Figure 21: Geometric model of machining step 9



Figure 22: Eccentric shaft after machining

Grooves were made along the  $\varnothing 80$  mm sections for retaining rings, after turning the eccentric shaft. Also, keyways were cut along the  $\varnothing 50$  mm section as shown in Figure 23. Knurling operation along the  $\varnothing 80$  mm section of the eccentric shaft is depicted in Figure 24.

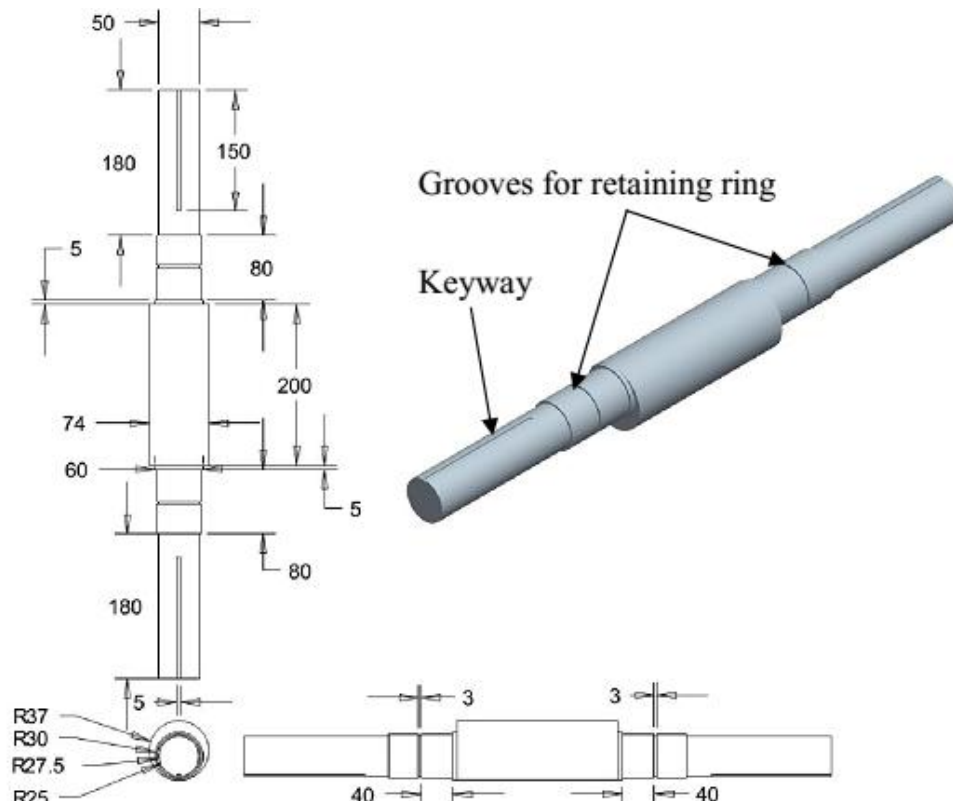


Figure 23: Third angle orthographic and isometric projections of the eccentric shaft with keyways and grooves for retaining rings



Figure 24: Knurling of the bearing part of the eccentric shaft for force fitting

## 2.5 Development of Hardfaced Jaws

The fixed and movable jaws of the jaw crusher were developed by welding a ferro-alloy hardfacing insert to mild steel substrate using manual metal arc welding at a welding speed of 120 mm/min and current of 100 A. Stringer hardfacing pattern of the insert was used to form the corrugations, while dot hardfacing pattern was made along the groove to protect the base plate as shown in Figure 25. The hardfacing insert contains mainly 72.8 % Fe, 12.32 % Mn, 7.38 % Cr and 4.35 % C. Detailed hardfacing procedures have been presented by Okechukwu *et al.* (2018). Geometric models of the movable and fixed hardfaced jaws are shown in Figure 26 and Figure 27, respectively.

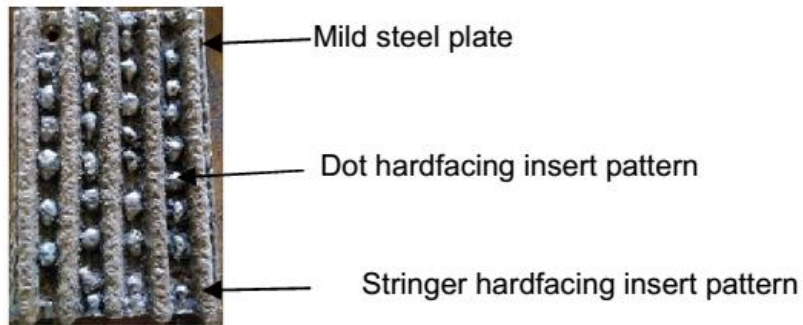


Figure 25: Hardfacing of mild steel with hardfacing insert to form hardfaced jaw (Okechukwu et al., 2018)

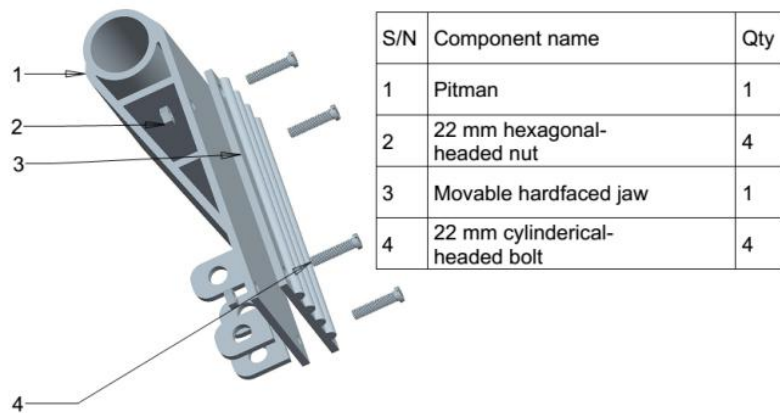


Figure 26: Exploded view of the pitman-movable jaw sub-assembly

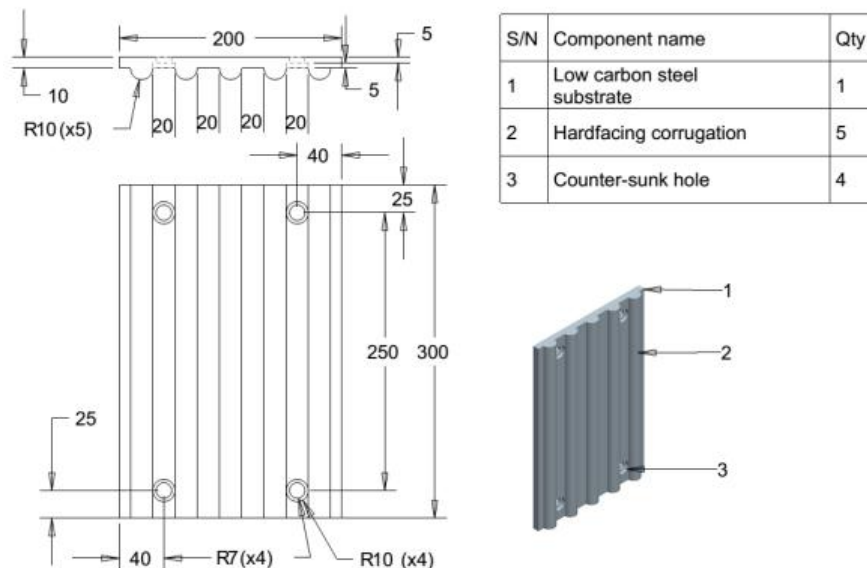


Figure 27: Fixed jaw-support plate sub-assembly and exploded view

## 2.6 Development of the Journal Bearings

The eccentric movement of pitman-movable jaw sub-assembly contributes significantly to the failure of bearings in jaw crushers. Frequent replacement of the bearing results in longer downtimes in quarries; hence, the journal bearings are critical components. Based on the eccentric diameter of the eccentric shaft and the bore diameter in the hubs of the pulley and flywheel, a decision was made to use a bearing whose bore diameter falls between the two diameters. This led to the selection and purchasing of four 6311-2RSC3 ball bearings, with  $\text{Ø}55$  mm internal diameter,  $\text{Ø}120$  mm external diameter and 29 mm thickness.

Consequently, a steel pipe of internal diameter  $\text{Ø}120$  mm, external diameter  $\text{Ø}140$  mm and length 200 mm was used to form the bearing housing, while 10 mm thick mild steel plate was used as the journal bearing base. Arc welding was used in joining the bearing housing to base plate and end plates. Exploded view of the journal bearing is presented in Figure 28.

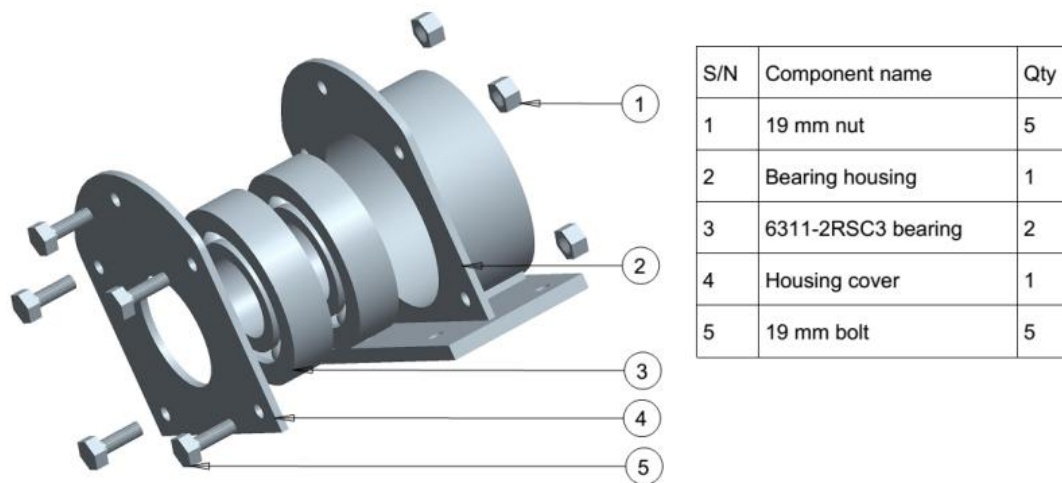


Figure 28: Exploded view of the journal bearing sub-assembly

## 2.7 Assembling of Jaw Crusher Components

The assembling sequence of the single toggle jaw crusher is summarized in steps A to D and the corresponding geometric models are presented in Figure 29 to 32. Assembling steps are as follow:

Step A: Crushing chamber was positioned on the base frame and fastened with bolts and nuts

Step B: Cheek plates were attached to inner side walls; thereafter, fixed jaw-support plate sub-assembly was fastened adjacent the cheek plates, while the toggle socket was attached opposite the fixed jaw

Step C: The pitman-movable jaw sub-assembly was hung on the eccentric shaft, the journal bearings were positioned on the eccentric shaft, and the toggle plate was attached to the lower end of the pitman prior to positioning the journal bearings on their sitting positions on the crushing chamber. The drawback rod was attached to the lower end of the pitman before the fastening of the compression spring to the back of the crushing chamber.

Step D: The 5 hp electric motor was fastened to the base frame; the  $\text{Ø}400$  mm pulley and flywheel were positioned on the eccentric shaft and secured with taper keys, while the  $\text{Ø}102$  mm pulley was also secured with a taper key. The pulleys were connected with two B82 V-belts.

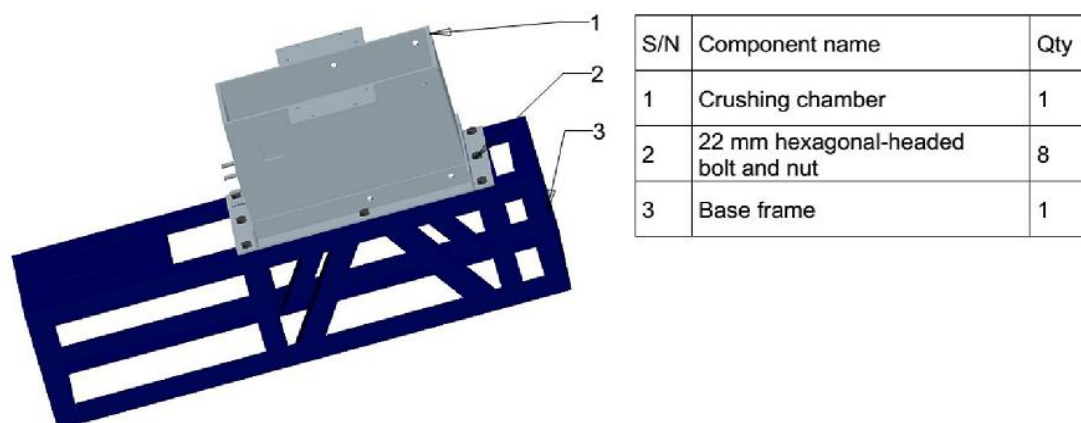


Figure 29: Geometric model of assembling step A

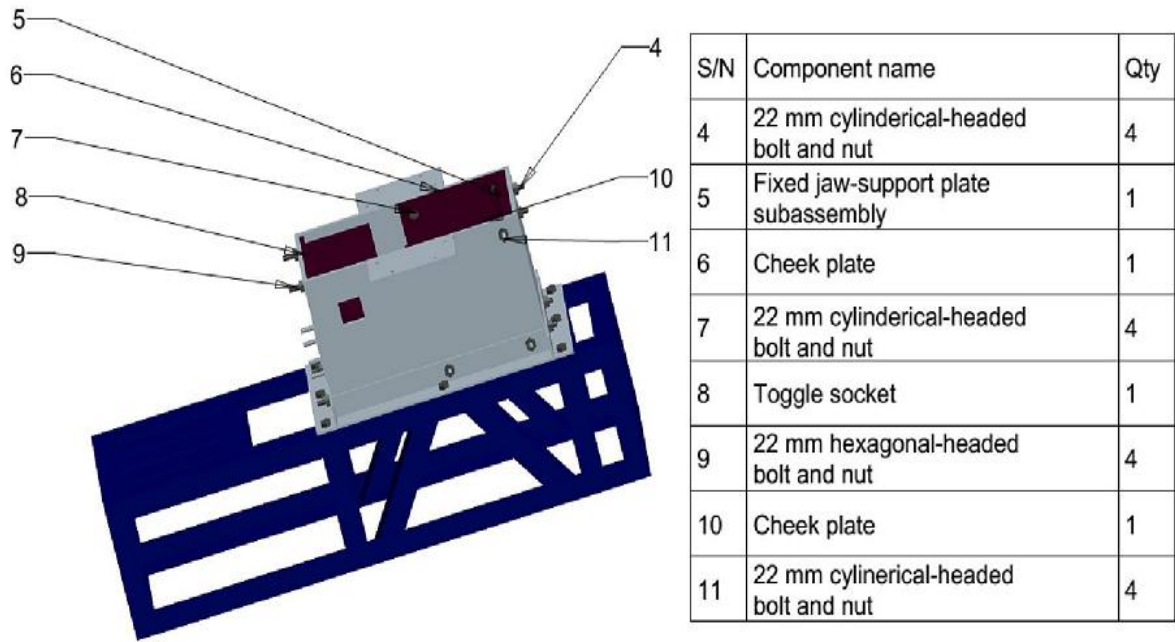


Figure 30: Geometric model of assembling step B

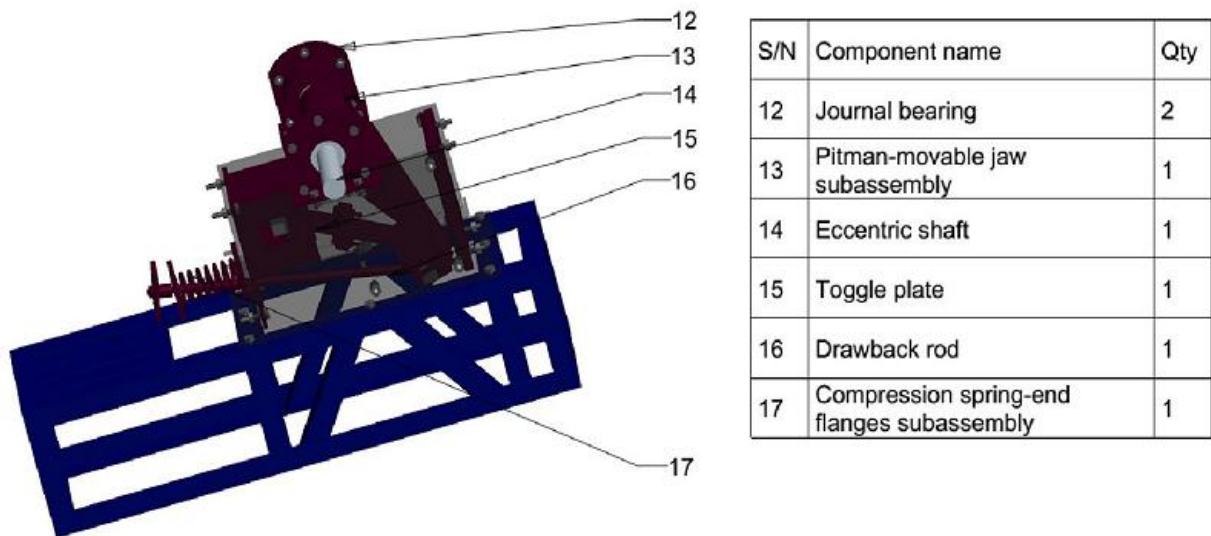


Figure 31: Geometric model of assembling step C

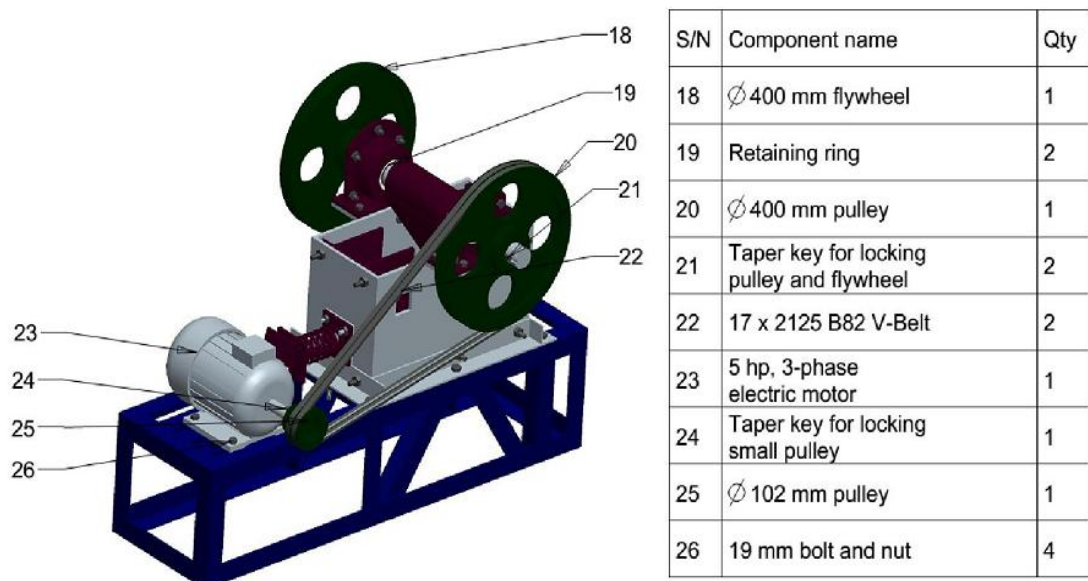


Figure 32: Geometric model of assembling step D

## 2.8 Determination of the Capacity of the Jaw Crusher

The crusher capacity was determined by crushing 80 kg of granite lumps with sizes ranging from 30 mm to 75 mm, and the crushing time in minutes was recorded.

## 2.9 Determination of the Variation of Eccentric Shaft Speed with Load

The effect of crushing varying quantities of granite on the eccentric shaft speed and the crusher stability was determined with the aid of a digital tachometer. Different quantities of the granite ranging from 0.1 kg to 0.6 kg were crushed and the corresponding eccentric shaft speeds were recorded.

## 3. Results and Discussion

### 3.1 Result of the Eccentric Shaft Design

Table 2 shows the results generated for the eccentric shaft when it was subjected to stress analysis in Autodesk Inventor®.

Table 2: Summary of Results of the Analysis of the Eccentric shaft

Design parameters	Symbol	Value
Maximal bending stress	$\sigma_B$	1.679 MPa
Maximal shear stress	$\tau_S$	0.254 MPa
Maximal torsional stress	T	0.896 MPa
Maximal deflection	$f_{max}$	9.323 microm
Angle of twist	$\Phi$	0.01 deg

The result showed that the angle of twist was insignificant; hence, there was no noticeable twisting in service. Shear force and bending moment diagrams of the eccentric shaft along the yz plane are presented in Figures 33 and 34, respectively.

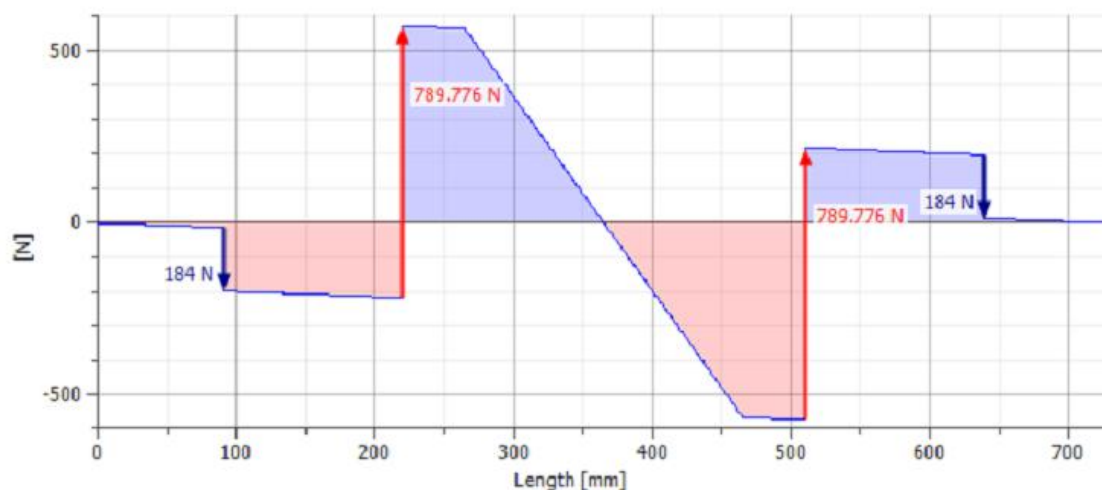


Figure 33: Shear force, yz plane

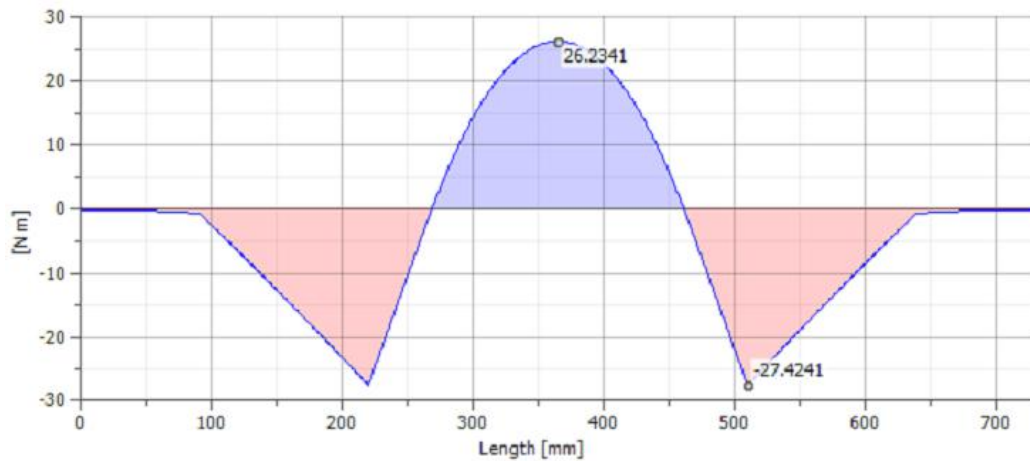


Figure 34: Bending moment , yz plane

From Figure 33, highest shear force value of 789.776 N occurred between the eccentric lobe and journal bearings. Maximum bending moment of magnitude 26.2341 Nm occurred at the centre of the eccentric shaft as presented in Figure 34.

### 3.2 Base Frame Stress Analysis

Static analysis of the base frame yielded the result shown in Table 3, while directional stiffness values are presented in Table 4. The directional stiffness values were calculated from the generated force and displacement.

Table 3: Result of Displacement of the Crusher Frame and Directional Forces

Name		Minimum	Maximum
Displacement		0.000 mm	0.008 mm
Forces	Fx	-139.376 N	578.346 N
	Fy	-321.792 N	586.004 N
	Fz	-103.447 N	400.771 N
Moments	Mx	-9892.886 N mm	10424.881 N mm
	My	-5768.540 N mm	9631.977 N mm
	Mz	-309.567 N mm	343.227 N mm
Normal Stresses	Smax	-0.648 MPa	4.158 MPa
	Smin	-5.678 MPa	0.012 MPa
	Smax(Mx)	0.000 MPa	3.256 MPa
	Smin(Mx)	-3.431 MPa	-0.000 MPa
	Smax(My)	0.000 MPa	3.170 MPa
	Smin(My)	-1.899 MPa	0.000 MPa
	Saxial	-0.860 MPa	0.222 MPa
Shear Stresses	Tx	-3.406 MPa	0.798 MPa
	Ty	-3.451 MPa	1.895 MPa
Torsional Stresses	T	-0.664 MPa	0.599 MPa

Table 4: Determination of Directional Stiffness

Force (N)	Max. displacement (mm)	Directional stiffness (N/mm)
Fx 578.346	0.008066	71,701.71
Fy 586.004	0.008066	72, 651.13
Fz 400.771	0.008066	49,686.46

The result of the frame's displacement when subjected to the weights of the crushing chamber accessories and the electric motor is shown in Figure 35. The frame is said to be statically stable or satisfactorily stiff considering the maximum displacement value of 0.008066 mm or 0.000008066 m, which is insignificant. High stiffness recorded can be attributed to the diagonal bracing below the crushing chamber position. These results are in agreement with the work reported by Rusiński et al. (2013), who posited that incorporating diagonal bracing inside a crusher frame increases the stiffness.

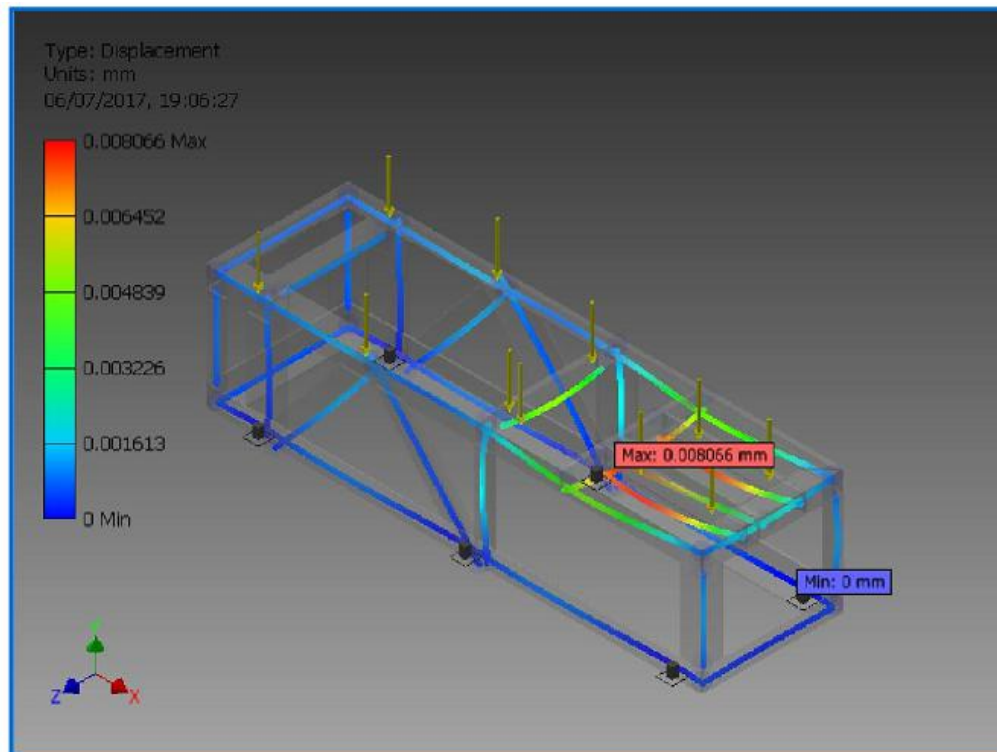


Figure 35: Static analysis result for the displacement of the jaw crusher base frame

The weakest part of the frame or the part with maximum displacement falls around the position of the electric motor-small pulley sub-assembly, where there is no diagonal bracing; the z-direction has the least stiffness as evidenced in Figure 36.

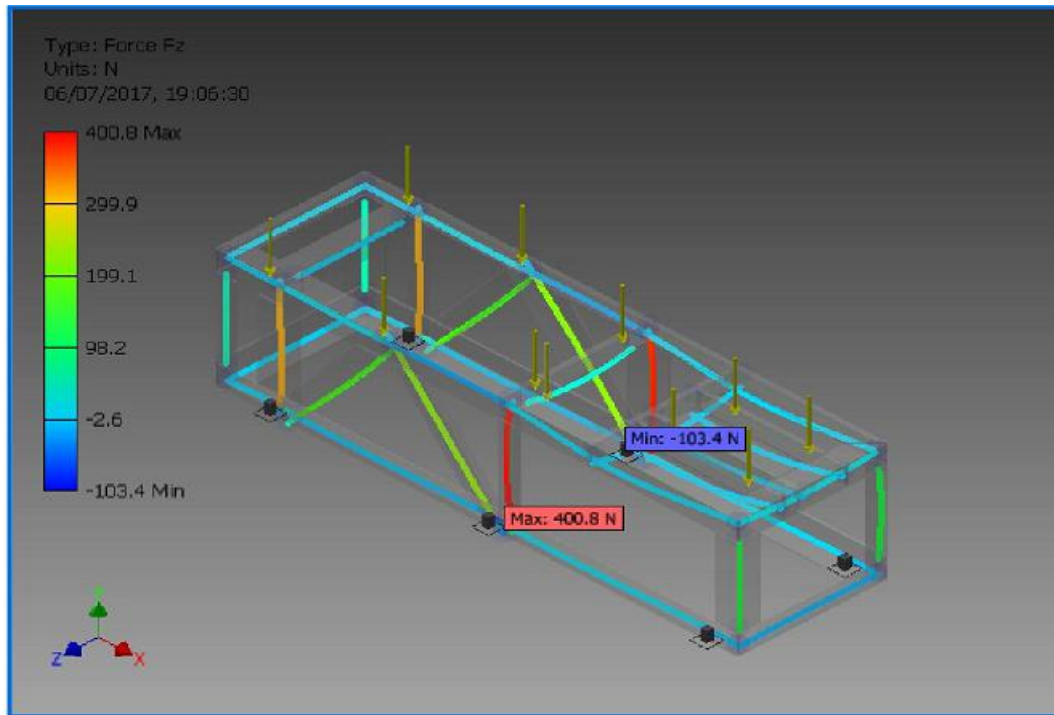


Figure 36: Force acting along z-direction due to components' weights

### 3.3 Result of the Spring Design

The results of the spring design are tabulated as shown in Table 5.

Table 5: Spring Design Parameters

Spring design parameters	Values
Spring constant	35.241 N/mm
Total spring deflection	17.026 mm
Spring limit force	2256.678 N
Endurance in shear	726.000 MPa
Min. load stress	178.149 MPa
Max. load stress	185.636 MPa
Critical speed of spring	14.600 mps
Natural frequency of spring surge	129.034 Hz
Spring check result	Positive

The spring check result is positive, indicating design compliance. It is clear that the spring will not fail when subjected to the forces specified. Furthermore, the spring index of 7.294 was within acceptable range of 4 to 12, while the total spring deflection of 17.026 mm favoured the designed crusher stroke of 5mm. Also, the spring limit force of 2256.678 N was greater than the total crushing force of 1683.62 N.

### 3.4 Capacity of the Jaw Crusher

The developed single toggle jaw crusher showing the evaluated hardfaced jaws and other critical components are shown in Figure 37.



Figure 37: Side and front views of the single toggle jaw crusher

After crushing the specified quantities of granite, the aggregate product size ranges from 5 mm to 15 mm, with majority falling around 12.5 mm. The average quantity of granite crushed, corresponding crushing time, and the calculated capacity of the crusher were 20kg, 5min and 0.24 ton/h, respectively.

The increased capacity beyond the designed capacity of 0.1 ton/hr can be attributed to the use of a higher horse power motor; this implies increased feed rate and throughput. Variation in the crushing time despite crushing the same quantity was due to voltage fluctuation, shape of granite lumps, friction and heat between the metal parts. It was observed that wedge-shaped granite lumps were easily nipped and crushed, while irregular-shaped lumps took longer crushing time.

### 3.5 Variation of Eccentric Shaft Speed with Load

Result of the analysis of effect of crushing increasing quantities of granite on the eccentric shaft speed of the jaw crusher is shown in Figure 38.

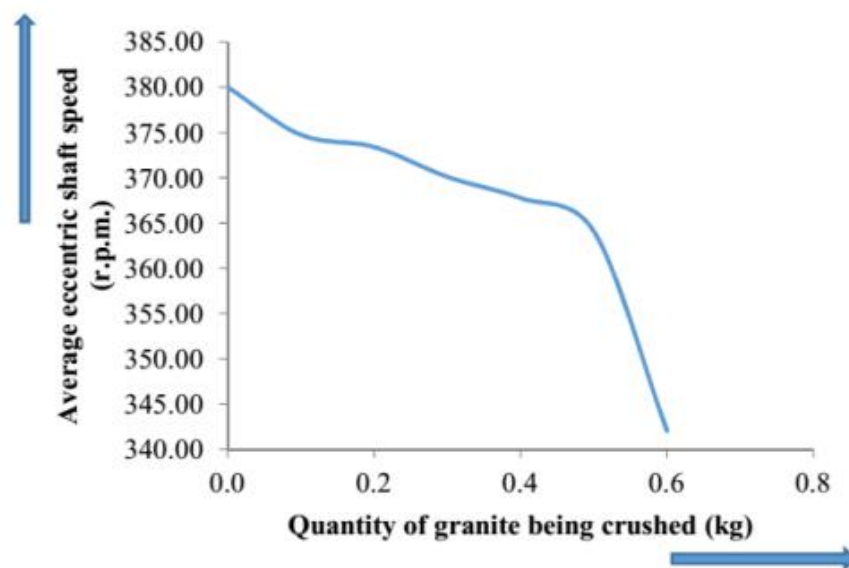


Figure 38: Variation of average eccentric shaft speed with quantity of granite crushed by the jaw crusher

From Figure 38, it is clear that the speed of the eccentric shaft decreases with increasing quantity of granite undergoing crushing in the crushing compartment of the laboratory size jaw crusher.

The shaft speed decreases more when the stone shape is irregular; hence, a longer crushing time as observed earlier during the capacity determination.

Furthermore, it was observed that the higher the quantity of granite undergoing crushing, the higher the noise and vibration of the crusher parts; this imposes stress on the electric motor. Crushing of 1 kg of granite resulted in an average eccentric shaft speed of 340.30 r.p.m. and a near breaking stress on the motor; hence, 1 kg was taken as the maximum load.

Additionally, a moderate load of 0.5 kg will ensure reduced stress on the electric motor and other components since there was a sharp drop in the shaft speed when 0.6 kg of granite was undergoing crushing.

#### **4. Conclusions**

Geometric modeling and stress analysis of the single toggle jaw crusher were achieved with Pro/Engineer® and Autodesk Inventor® softwares, respectively. Stress analysis revealed that both the angle of twist of the eccentric shaft,  $0.01^\circ$  and the maximum displacement of the base frame, 0.008066 mm, were insignificant; also, spring check result was positive and summarily indicated design compliance.

Method of developing critical components of the jaw crusher such as: eccentric shaft, by welding a removable offset shaft before machining; journal bearing, by the use of fabricated journal housing and detachable ball bearings; and crusher jaws, by hardfacing ferro-alloy hardfacing alloy inserts to low carbon steel substrate, were found economical for easy repairs and replacement.

Performance evaluation of the machine showed that the actual capacity of the crusher was higher than the design capacity, owing to the selection of a higher capacity electric motor as prime mover. It was observed that the average speed of the eccentric shaft decreased with increasing mass of granite undergoing crushing and when crushing irregular-shaped than wedge-shaped lumps of granite. The methods used in developing the critical components of the jaw crusher can be adopted in developing affordable jaw crushers for artisanal miners and stone workers. More so, these offer shorter reparation time and will reduce the proliferation of moribund quarries in Nigeria.

#### **Recommendation**

The methods used in developing the critical components of the single toggle jaw crusher are sustainable and should be adopted by machine builders to boost the productivity and livelihood of artisanal miners and stones workers, and increase the profitability of small and medium scale enterprises in the minerals sector.

#### **Acknowledgement**

The authors are grateful to the management and technical staff of Advanced Manufacturing Technology Programme, Jalingo, Taraba State, Scientific Equipment Development Institute, Enugu, Enugu State, Union Foundry Industries, Port Harcourt, Rivers State and M. K. Technical Enterprises, Jalingo, Taraba State, Nigeria, for their technical assistance in the course of this research.

#### **References**

Alonge, A. 2015. Development of a prototype jaw-type rock crushing machine. M. Eng. Thesis, Department of Mechanical Engineering, Federal University of Technology, Akure, Ondo State, Nigeria.

Asbjörnsson, G. 2013. Modelling and simulation of dynamic behaviour in crushing plants. Thesis for the Degree of Licentiate of Engineering, Department of Product and Production Development Department, Chalmers University of Technology, Göteborg, Sweden.

- Birabwa, E. 2006. Small-scale stone quarrying: Its contribution to people's livelihoods. A case study of Kesange Parish, Nama Sub-County, Mukuno District, Uganda. M. Phil. Thesis, Department of Geography, Norwegian University of Science and Technology, Trondheim.
- Donovan, JG. 2003. Fracture toughness based models for the prediction of power consumption, product size and capacity of jaw crushers. Ph. D. Dissertation, Mining and Minerals Engineering, Faculty of Virginia Polytechnic Institute and State University, Blacksburg, VA.
- Elisante, E. 2009. Simplification of jaw crusher for artisanal aggregate miners. Journal of Engineering and Technology Research, 1(6):102-108.
- Juvinall, RC. and Marshek, KM. 2012. Fundamentals of machine component design. 5th ed.: John Wiley & Sons, Inc., New Jersey.
- Karra, VK., Magerowski, AJ. and Szalanski, SE. 1992. Method of high performance jaw crushing. US Patent No. 5,110,057.
- Kelly, EG. and Spottiswood, DJ. 1992. Introduction to mineral processing. John Wiley and Sons, Inc., Canada.
- Khurmi, RC. and Gupta, JK. 2005. A textbook of machine design. Eurasia Publishing House (Pvt.) Ltd, New Delhi.
- Mohamed, A., Gilbert, G. and Nicholas, M. 2014. Mechanical design of a small scale mechanized stone crusher. Bachelor Degree Thesis, Department of Mechanical and manufacturing Engineering, University of Nairobi.
- More, RS. and Rajpal, SJ. 2013. A review on the study of jaw plates of jaw crusher. International Journal of Modern Engineering Research, 3(1):518-522.
- Niemela, R. and Kieranen, C. 2008. Portable apparatus for crushing rock and other hard materials and related method. US Patent No. 7,448,564 B2.
- Norton, RL. 2000. Machine design: an integrated Approach. Prentice-Hall Inc, New Jersey.
- Numbi, BP., Zhang, J. and Xia, X. 2014. Optimal energy management for a jaw crushing process in deep mines. Energy, 68:337-348.
- Okechukwu, C., Dahunsi, OA., Oke, PK., Oladele, IO., and Dauda, M. 2018. Development of hardfaced crusher jaws using ferro-alloy hardfacing inserts and low carbon steel substrate. Jurnal Tribologi, 18:20-39.
- Pokrajcic, Z. 2010. Advanced comminution circuit design – essential for industry. Mineral Processing Bulletin. Metso, pp. 38-42.
- Ravindran, S. 2010. Stone crushers and dust problem. Middle-East Journal of Scientific Research, 14(12):1734-1740.
- Rusiński, E., Moczko, P., Pietrusiak, D., and Przybyłek, G. 2013. Experimental and numerical studies of jaw crusher supporting structure fatigue failure. Strojniški Vestnik – Journal of Mechanical Engineering, 59(9):556-563.
- UNDP. 2014. Framework for harnessing the extractive industries for inclusive growth and development in Nigeria. United Nations Development Programme, Abuja, Nigeria.
- Waguespack, C. 2013. Mastering Autodesk® Inventor® 2014 and Autodesk® Inventor LTTM. John Wiley and Sons, Inc, Indiana.
- Wills, BA. 2016. Mineral processing technology: an introduction to the practical aspects of ore treatment and mineral recovery. Elsevier, London.
- Zhang, J. 2014. Particle technology-study notes. <http://lorien.ncl.ac.uk/ming/particle/cpe124p4.html>, accessed on 09 September, 2014.